Available online at www.sciencedirect.com
SCIENCE DIRECT
Advances in Water Resources 29 (2006) 1196–1208
Advances in Water Resources
www.elsevier.com/locate/advwatres

Velocity distribution in combined wave–current flows

Shu-Qing Yang [a,*], Soon-Keat Tan [b], Siow-Yong Lim [c], Shuo-Fu Zhang [d]

[a] Division of Civil and Environmental Engineering, Korea Maritime University, Busan 606791, Republic of Korea
[b] Maritime Research Center, Nanyang Technological University, Singapore 639798, Singapore
[c] School of Civil and Environmental Engineering, Nanyang Technological University, Singapore 639798, Singapore
[d] Bureau of Water Resources of Hunan Province, Changsha 410082, China

Received 27 April 2004; received in revised form 8 August 2005; accepted 28 September 2005
Available online 17 November 2005

Abstract

This paper investigates why the measured velocity profiles in combined wave–current flows deviate from the log-law. Most of previous researchers attributed the velocity deviation to the wave Reynolds stress—$\rho\tilde{\bar{u}}\tilde{\bar{v}}$ only. However, this study shows that both the wave Reynolds stress and the momentum $\bar{u}\bar{v}$ driven by secondary flow and/or non-uniformity are responsible to the velocity deviation from the log-law. The theoretical investigation starts from the Reynolds equations and uses the simplified mixing-length hypothesis. The theoretical equation which describes the interaction of velocity distribution and $\bar{v}$ in combined wave and current conditions from the bottom to the free surface is obtained, and the equation states that the non-zero wall-normal velocity $\bar{v}$ that has been ignored in previous studies also plays an important role as the wave Reynolds stress to the velocity profile. By comparing the model with the available experimental data, it is seen that the model predicted the essential features of the experimental results.

Keywords: Velocity distribution; Wave–current flow; Karman constant; Bed shear stress; Wave Reynolds shear stress; Wall-normal velocity

1. Introduction

The velocity distribution in combined wave–current flows is important for determination of sediment transport in coastal waters, wave height attenuation, pollution control, wave–current interactions, and so on. There are as yet limited number of experimental and theoretical studies on the velocity distribution in the combined wave–current conditions probably because experimental equipment of unsteady flows and the measurement techniques are much more difficult than those of steady flows. The observed velocity distribution in the combined wave–current flows and other flows such as the boundary layer flows, steady and non-uniform open channel flows are such that the measured Reynolds shear stress and velocity distribution are different from those in circular pipe flows ([3,8], etc.), and the classic log-law that has been well accepted by many researchers from Keulegan's [11] era. The experimental results in the combined wave–current flows ([1,9,19,23], etc.) show that the current velocity increases logarithmically from the seabed, reaches the maximum value and then decreases towards the free surface when the waves and current propagate in the same direction. The converse was observed by Kemp and Simons [10] in the flows in which the waves propagate against the current.

In short, the velocity distribution in the wave–current flows follows the log-law near the seabed and the relative directions of flow do not influence the interaction near the bed. In the upper layer mean velocities are either larger or smaller than that predicted using the log-law, and are dependent on the direction of wave propagation. One difficulty for anyone attempting to model the interaction of wave and current is that there are relatively fewer

* Corresponding author. Tel.: +82 51 4104466; fax: +82 51 4104415.
E-mail addresses: csqyang@ntu.edu.sg (S.-Q. Yang), ctansk@ntu.edu.sg (S.-K. Tan), csylim@ntu.edu.sg (S.-Y. Lim).

0309-1708/$ - see front matter © 2005 Elsevier Ltd. All rights reserved.
doi:10.1016/j.advwatres.2005.09.010

Nomenclature

a	coefficient
b	$1 - gh(\sin\theta + S)/u_*^2 - ah/u_*^2$
c	integration constant
g	gravitational acceleration
h	water depth
H	wave height
k	wave number
m	coefficients
n	coefficients
N	number of wave
p	pressure
$Q_{(y)}$	total energy at elevation y
S	energy slope
T	wave period
u_*	shear velocity
u, v and w	velocities in x, y and z directions, respectively
u_r	reference current velocity at y_r
V	depth mean velocity
V	depth-averaged velocity
x	streamwise direction
y	distance to channel bed
y_{max}	distance from the level of maximum velocity to the bed
y_0	reference level
y_0	$\Delta/30$ for a rough wall
y_0	$\nu/(9.9u_*)$ for smooth wall
z	lateral direction
$\overline{\tilde{v}_h^2}$	oscillatory vertical velocity at free surface
$\overline{u'v'}$	Reynolds shear stress
$\bar{u}\bar{v}$	shear stress caused by mean velocities
$\overline{\tilde{u}\tilde{v}}$	shear stress caused by waves
$\bar{p}_0$	time-averaged pressure at the bed
$\bar{p}_h$	water pressure at free surface
$\bar{u}$ and $\bar{v}$	time-averaged velocities
u' and v'	velocity fluctuation caused by turbulence
$\tilde{u}$ and $\tilde{v}$	velocity fluctuation caused by waves
Δ	boundary roughness height
$\bar{v}_{y=h}$ and $\bar{u}_{y=h}$	wall-normal and streamwise velocities at the free surface
α	coefficients
β	momentum correction factor
θ	angle of the channel bed to the horizontal axis
κ	Karman constant
ν	kinematic viscosity of the fluid
ξ	y/h
ρ	fluid density
τ_0	bed shear stress
ω	angular wave frequency

measurements for this type of flow. Although considerable research has gone into the study of waves and currents as separate and independent process, little is known about the way in which they interact with each other.

Many attempts have been made to express the velocity in the combined wave–current flows, most previous models have assumed that wave-induced turbulence has similar characteristics to that of a steady flow. Therefore the eddy viscosity and mixing length obtained from the steady flows can be directly applied to combined wave–current flow. Lundgren [14] and many later researchers had developed models based on the ideas that the current profile is logarithmic along the wave boundary layer. However, the observed increase or decrease of the current velocity relative to a logarithmic profile cannot be explained fully using the existing analytical models, such as those proposed by Grant and Madsen [5], Fredsoe [4], Christoffersen and Jonsson [2], Sleath [20], Groeneweg and Klopman [6] and Groeneweg and Battjes [7].

A number of models have included velocity distortion in the upper flow layer. You [30] stressed that the wave Reynolds shear stress plays a significant role on the deviation of measured velocity from that given by the classical log-law. You's model gives reasonably good match of the velocity profile from the seabed to the free surface. Sleath [20], on the other hand, argued that the wave-induced turbulence is similar to those of grid-generated turbulence and he suggested that the turbulence fluctuation in the vertical direction $\overline{v'^2}$ plays an important role for the velocity distribution. Yang [28] reanalyzed the velocity profiles in sediment-laden flows, steady open channel flows as well as the zero-pressure-gradient boundary layers flows and concluded that all phenomenon of velocity deviation from the log-law can be attributed to the non-zero wall-normal velocity.

The objectives of the present study are (1) to establish the momentum equation in the combined wave–current flows; (2) to investigate the influence of wall-normal velocity on the streamwise velocity, and (3) to put forward a new model of velocity profile under combined wave and current.

2. Governing equations for fluid motions

The velocity distribution in unsteady flows is of great interest in practice. The governing equations for flows in coastal waters are the conservation of mass and Navier–Stokes equations as follows:

$$\frac{\partial u}{\partial x}+\frac{\partial v}{\partial y}+\frac{\partial w}{\partial z}=0 \tag{1}$$

$$\frac{\partial u}{\partial t}+u\frac{\partial u}{\partial x}+v\frac{\partial u}{\partial y}+w\frac{\partial u}{\partial z}=-\frac{1}{\rho}\frac{\partial p}{\partial x}+\nu\left(\frac{\partial^2 u}{\partial x^2}+\frac{\partial^2 u}{\partial y^2}+\frac{\partial^2 u}{\partial z^2}\right)+g\sin\theta \tag{2}$$

$$\frac{\partial v}{\partial t}+u\frac{\partial v}{\partial x}+v\frac{\partial v}{\partial y}+w\frac{\partial v}{\partial z}=-\frac{1}{\rho}\frac{\partial p}{\partial y}+\nu\left(\frac{\partial^2 v}{\partial x^2}+\frac{\partial^2 v}{\partial y^2}+\frac{\partial^2 v}{\partial z^2}\right)-g\cos\theta \tag{3}$$

$$\frac{\partial w}{\partial t}+u\frac{\partial w}{\partial x}+v\frac{\partial w}{\partial y}+w\frac{\partial w}{\partial z}=-\frac{1}{\rho}\frac{\partial p}{\partial z}+\nu\left(\frac{\partial^2 w}{\partial x^2}+\frac{\partial^2 w}{\partial y^2}+\frac{\partial^2 w}{\partial z^2}\right) \tag{4}$$

where u, v and w are velocities in x, y and z directions, respectively; ρ is the fluid density; p is the pressure; and ν is the kinematic viscosity of the fluid; x is the streamwise direction; y is perpendicular to the channel bed and z is the lateral direction; g is the gravitational acceleration; θ is the angle of the channel bed to the horizontal axis as shown in Fig. 1.

The following equations are obtained by adding the continuity equation to the momentum equations

$$\frac{\partial u}{\partial t}+\frac{\partial uu}{\partial x}+\frac{\partial uv}{\partial y}+\frac{\partial uw}{\partial z}=-\frac{1}{\rho}\frac{\partial p}{\partial x}+\nu\left(\frac{\partial^2 u}{\partial x^2}+\frac{\partial^2 u}{\partial y^2}+\frac{\partial^2 u}{\partial z^2}\right)+g\sin\theta \tag{5}$$

$$\frac{\partial v}{\partial t}+\frac{\partial uv}{\partial x}+\frac{\partial vv}{\partial y}+\frac{\partial vw}{\partial z}=-\frac{1}{\rho}\frac{\partial p}{\partial y}+\nu\left(\frac{\partial^2 v}{\partial x^2}+\frac{\partial^2 v}{\partial y^2}+\frac{\partial^2 v}{\partial z^2}\right)-g\cos\theta \tag{6}$$

$$\frac{\partial w}{\partial t}+\frac{\partial wu}{\partial x}+\frac{\partial vw}{\partial y}+\frac{\partial ww}{\partial z}=-\frac{1}{\rho}\frac{\partial p}{\partial y}+\nu\left(\frac{\partial^2 w}{\partial x^2}+\frac{\partial^2 w}{\partial y^2}+\frac{\partial^2 w}{\partial z^2}\right) \tag{7}$$

Similar to the classical Reynolds equations for a steady turbulent flow in which the instantaneous velocity is expressed as the sum of mean velocity and velocity fluctuation, the velocity in a wave–current flow includes a steady mean velocity, a periodic component and a random velocity (primed term) fluctuation, i.e.,

$$(u,v,w)=(\bar{u}+\tilde{u}+u',\bar{v}+\tilde{v}+v',\bar{w}+\tilde{w}+w') \tag{8}$$

The periodic component is the phase-average over N number of wave periods minus the time-averaged value, i.e.,

$$\tilde{u}=\frac{1}{N}\sum_{j=1}^{N}[u(t+jT)-\bar{u}] \tag{9}$$

where T is the wave period. Substituting Eq. (8) into Eqs. (5) and (6), noting that $\bar{\tilde{x}}=\bar{x'}=\tilde{x'}=0$, and $\overline{\tilde{x}\tilde{y}}=\bar{\tilde{x}}\bar{y'}=\bar{\tilde{x}}\widetilde{y'}\cong\bar{x}\widetilde{x'}=\widetilde{\tilde{x}y'}=0$, while $\widetilde{\tilde{x}\tilde{y}}=\tilde{x}\tilde{y}-\overline{\tilde{x}\tilde{y}}$, one obtains the governing equation for time-averaged velocities $\bar{u}$ and $\bar{v}$ as follows:

$$\frac{\partial}{\partial x}\left(\bar{u}^2+\overline{\tilde{u}^2}+\overline{u'^2}-\nu\frac{\partial\bar{u}}{\partial x}\right)+\frac{\partial}{\partial y}\left(\bar{u}\bar{v}+\overline{u'v'}+\overline{\tilde{u}\tilde{v}}-\nu\frac{\partial\bar{u}}{\partial y}\right)+\frac{\partial}{\partial z}\left(\bar{u}\bar{w}+\overline{u'w'}+\overline{\tilde{u}\tilde{w}}-\nu\frac{\partial\bar{u}}{\partial z}\right)=-\frac{1}{\rho}\frac{\partial\bar{p}}{\partial x}+g\sin\theta \tag{10}$$

$$\frac{\partial}{\partial x}\left(\bar{u}\bar{v}+\overline{\tilde{u}\tilde{v}}+\overline{u'v'}-\nu\frac{\partial\bar{v}}{\partial x}\right)+\frac{\partial}{\partial y}\left(\bar{v}^2+\overline{v'^2}+\overline{\tilde{v}^2}-\nu\frac{\partial\bar{v}}{\partial y}\right)+\frac{\partial}{\partial z}\left(\bar{v}\bar{w}+\overline{v'w'}+\overline{\tilde{v}\tilde{w}}-\nu\frac{\partial\bar{v}}{\partial z}\right)=-\frac{1}{\rho}\frac{\partial\bar{p}}{\partial y}-g\cos\theta \tag{11}$$

For simplicity, this study only discusses the two-dimensional ($\partial/\partial z=0$) wave–current flow with constant water depth. Considering the boundary conditions at the bed where $y=y_0,\bar{u}=\bar{v}=\overline{u'v'}=\overline{\tilde{u}\tilde{v}}=0$ and $\nu\partial\bar{u}/\partial y=\tau_0/\rho=u_*^2$, in which τ_0 is the bed shear stress and u_* is shear velocity, the integration of Eq. (10) with respect to y from y_0 to y yields:

$$\bar{u}\bar{v}+\overline{u'v'}-\nu\frac{\partial\bar{u}}{\partial y}+u_*^2=-\int_{y_0}^{y}\frac{\partial}{\partial x}\left(\frac{\bar{p}}{\rho}+\bar{u}^2+\overline{u'^2}+\overline{\tilde{u}^2}-\nu\frac{\partial\bar{u}}{\partial x}\right)\mathrm{d}y+gy\sin\theta-\overline{\tilde{u}\tilde{v}} \tag{12}$$

at the free surface where $y=$ water depth $=h$, $\bar{v}=0$ and the friction on the air–liquid interface is negligible, i.e., $\overline{u'v'}\approx 0$, $\nu\partial\bar{u}/\partial y\approx 0$. On the other hand, $\bar{u}^2\gg\overline{u'^2}$ and the viscous effect in the main flow region is negligible, or $\partial(\overline{u'^2}-\nu\partial\bar{u}/\partial x)/\partial x\approx 0$, thus the boundary shear stress can be determined using Eq. (12).

$$\frac{\tau_0}{\rho}=u_*^2=-\overline{\tilde{u}\tilde{v}}|_{y=h}-\int_{y_0}^{h}\frac{\partial}{\partial x}\left(\frac{\bar{p}}{\rho}+\bar{u}^2+\overline{\tilde{u}^2}\right)\mathrm{d}y+gh\sin\theta \tag{13}$$

The time-averaged pressure at an arbitrary level can be obtained from Eq. (11) with the boundary condition at the bed, $y=y_0$, $\bar{v}=\overline{v'}=\overline{\tilde{v}}=0$ and $\bar{p}=\bar{p}_0$,

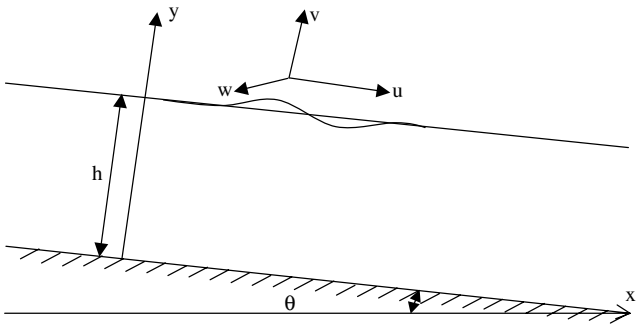

Fig. 1. Coordinate system in unsteady flows.

$$\frac{\bar{p}}{\rho}=\frac{\bar{p}_0}{\rho}-gy\cos\theta-\left(\bar{v}^2+\overline{v'^2}+\overline{\tilde{v}^2}-\nu\frac{\partial\bar{v}}{\partial y}\right)-\frac{\partial}{\partial x}\int_{y_0}^{y}\left(\bar{u}\bar{v}+\overline{\tilde{u}\tilde{v}}+\overline{u'v'}-\nu\frac{\partial\bar{v}}{\partial x}\right)\mathrm{d}y \tag{14}$$

in which $\bar{p}_0$ is the time-averaged pressure at the bed and it can be determined from Eq. (14) using the free surface conditions at $y=h$, $\bar{p}=\bar{p}_h$, $\bar{v}=0$, $\overline{v'^2}\approx 0$. The viscous effect near the free surface is also negligible, i.e., $\nu\partial\bar{v}/\partial y\approx 0$

$$\frac{\bar{p}_0}{\rho}=\frac{\bar{p}_h}{\rho}+gh\cos\theta+\overline{\tilde{v}_h^2}+\int_{y_0}^{h}\frac{\partial}{\partial x}\left(\bar{u}\bar{v}+\overline{\tilde{u}\tilde{v}}+\overline{u'v'}-\nu\frac{\partial\bar{v}}{\partial x}\right)\mathrm{d}y \tag{15}$$

where $\bar{p}_h$ and $\overline{\tilde{v}_h^2}$ are water pressure and oscillatory vertical velocity at free surface, respectively. Substituting Eq. (15) into (14) leads to

$$\frac{\bar{p}}{\rho}=\frac{\bar{p}_h}{\rho}+g(h-y)\cos\theta+\overline{\tilde{v}_h^2}-\left(\bar{v}^2+\overline{v'^2}+\overline{\tilde{v}^2}-\nu\frac{\partial\bar{v}}{\partial y}\right)+\int_{y}^{h}\frac{\partial}{\partial x}\left(\bar{u}\bar{v}+\overline{\tilde{u}\tilde{v}}+\overline{u'v'}-\nu\frac{\partial\bar{v}}{\partial x}\right)\mathrm{d}y \tag{16}$$

Substituting Eq. (16) into (12) and ignoring the viscous shear stress, one gets

$$\bar{u}\bar{v}+\overline{u'v'}+u_*^2=gy\sin\theta-\int_{y_0}^{y}\frac{\partial Q_{(y)}}{\partial x}\mathrm{d}y-\overline{\tilde{u}\tilde{v}}-\int_{y_0}^{y}\frac{\partial}{\partial x}\int_{y}^{h}\frac{\partial}{\partial x}\left(\bar{u}\bar{v}+\overline{\tilde{u}\tilde{v}}+\overline{u'v'}-\nu\frac{\partial\bar{v}}{\partial x}\right)\mathrm{d}y^2 \tag{17}$$

where $Q_{(y)}$ is the total energy at elevation y and can be expressed as follows:

$$Q_{(y)}=\frac{\bar{p}_h}{\rho}+g(h-y)\cos\theta+\overline{\tilde{v}_h^2}+\bar{u}^2-\bar{v}^2+\overline{u'^2}-\overline{v'^2}+\overline{\tilde{u}^2}-\overline{\tilde{v}^2} \tag{18a}$$

where $\bar{p}_h$ is the time-averaged pressure on the mean water level, and it is caused by atmospheric pressure as well as wave action, for combined wave–current flows $\bar{p}_h$ is greater than the atmospheric pressure due to the additional wave pressure, and $\bar{p}_h$ depends on the wave period and wave height. It is obvious for steady flow without waves superimposed that $\bar{p}_h=$ atmospheric pressure $=$ constant; all parameters related to waves vanish; and notice that $\bar{u}^2\gg\bar{v}^2+\overline{v'^2}-\overline{u'^2}$, therefore the second term on right-hand-side (RHS) of Eq. (17) becomes

$$\int_{y_0}^{y}\frac{\partial Q_{(y)}}{\partial x}\mathrm{d}y\approx gy\frac{\partial h}{\partial x}\cos\theta+\int_{y_0}^{y}\frac{\partial\bar{u}^2}{\partial x}\mathrm{d}y\approx gy\left(\frac{\Delta h+\beta\Delta V^2}{\Delta x}\right)=gSy \tag{18b}$$

where $\beta=$ momentum correction factor; $V=$ depth mean velocity and $S=$ energy slope. Similarly, for combined wave–current flows the term of $-\partial Q/\partial x$ represents the energy loss along the streamwise direction. Thus the second term on the RHS of Eq. (17) can be written as:

$$-\int_{y_0}^{y}\frac{\partial Q_{(y)}}{\partial x}\mathrm{d}y=gyS \tag{19}$$

Obviously, for Airy waves, S mainly relys on the variation of water depth because the discharge Vh is constant and the discharge from the wave trough to the wave crest is negligible relative to the total discharge.

The third term on the RHS of Eq. (17) is the wave-induced Reynolds stress that is related to the velocities driven by waves. Its maximum value generally occurs at the free surface. Nielsen and You [16] derived the distribution of the expression outside the laminar wave boundary layer, Rivera and Arcilla [17] obtained the wave Reynolds stress distribution based on the concept of vorticity and the continuity equation. Experimental data [18] show that the wave Reynolds stress distribution is linear. You [30] analyzed the measured wave Reynolds stress and concluded that the measured wave Reynolds does not follow Longuet-Hinggins [13] equation, but a linear function, i.e.,

$$\overline{\tilde{u}\tilde{v}}=ay \tag{20a}$$

$$a=\frac{\kappa|u_*|\left(\bar{u}_r-\frac{\bar{u}_*}{\kappa}\ln\frac{y_r}{y_0}\right)}{h\ln(1-y_r/h)}+\frac{\partial H}{\partial x}\frac{H\omega^2}{4\sinh^2 kh} \tag{20b}$$

where $\kappa=0.4$; $H=$ wave height; $\omega=$ angular wave frequency; $u_*=$ shear velocity; $u_r=$ reference current velocity at y_r, $k=$ wave number.

The last term in RHS of Eq. (17) is negligible [30]. Therefore, inserting Eqs. (18)–(20) into (17), one obtains

$$\bar{u}\bar{v}+\overline{u'v'}+u_*^2=gy\sin\theta+gSy+ay \tag{21}$$

Eq. (21) can be rewritten as follows:

$$\frac{-\overline{u'v'}}{u_*^2}=\left(1-\frac{y}{h}\right)+b\frac{y}{h}+\frac{\bar{u}\bar{v}}{u_*^2} \tag{22}$$

where b is independent of vertical distance y and $b=1-gh(\sin\theta+S)/u_*^2-ah/u_*^2$.

Although Eq. (22) is derived from the combined wave–current flows, its application covers steady and uniform flows, steady and non-uniform flows and unsteady flows, for example: in circular pipe flows $b=0$ and $v=0$; in steady, uniform and fully developed straight channel flows, $a=0$.

The Reynolds shear stress is often modeled by the mixing-length hypothesis as follows:

$$-\overline{u'v'}=(\kappa y)^2\left(\frac{\mathrm{d}\bar{u}}{\mathrm{d}y}\right)^2 \tag{23a}$$

where $\kappa =$ Karman constant ≈ 0.4. Note that experimental results show that Eq. (23a) is only valid near the boundary [15]. The modified Reynolds shear stress is often expressed by the following empirical equation [27, p. 202]

$$-\overline{u'v'} = \kappa u_* y(1-\xi)\frac{\mathrm{d}\bar{u}}{\mathrm{d}y} \tag{23b}$$

where $\xi = y/h$. In this study, Eq. (23b) is used to model the Reynolds shear stress.

3. Analytical solutions of velocity distribution in non-uniform and unsteady flows

By inserting Eq. (23b) into (22), the following equation is obtained:

$$\frac{\bar{u}}{u_*} = \exp\left(\int \frac{\bar{v}\,\mathrm{d}\xi}{\kappa u_* \xi(1-\xi)}\right)\left[\int \exp\left(\int \frac{-\bar{v}\,\mathrm{d}\xi}{\kappa\xi u_*(1-\xi)}\right) \times\left(\frac{1}{\kappa\xi}+\frac{b}{\kappa(1-\xi)}\right)\mathrm{d}\xi + c\right] \tag{24}$$

where c is the integration constant, and is determined by the non-slip boundary condition, i.e., at $y = y_0$, $\bar{u} = 0$.

If $\bar{v} = 0$, Eq. (24) gives

$$\frac{\bar{u}}{u_*} = \frac{1}{\kappa}\ln\frac{y}{y_0} - \frac{b}{\kappa}\ln(1-\xi) \tag{25}$$

Eq. (25) is similar to the formula developed by You [30] who obtained it using a different approach in wave–current combined flows, assuming that $a \neq 0$. The classical log-law can be derived if $b = 0$. This indicates that the log-law is valid only when b and $\bar{v}$ are negligible, viz.

$$\frac{\bar{u}}{u_*} = \frac{1}{\kappa}\ln\frac{y}{y_0} \tag{26}$$

For a smooth wall, $y_0 = \nu/(9.9u_*)$ and $\nu =$ kinematic viscosity; for a rough wall, $y_0 = \Delta/30$ and $\Delta =$ the boundary roughness height.

Eq. (25) shows that the maximum velocity appears below the free surface. At the point of maximum velocity, the velocity gradient is zero, i.e., $\mathrm{d}\bar{u}/\mathrm{d}y = 0$, thus, one gets the following equation from Eq. (25):

$$b = 1 - \frac{h}{y_{\max}} \tag{27}$$

where $y_{\max} =$ the distance from the level of the maximum velocity to the bed. Obviously, if the maximum velocity occurs on the free surface, i.e., $y_{\max} = h$, then $b = 0$ and Eq. (26) states that the velocity profiles follow the log-law, otherwise $y_{\max} < h$ or $b < 0$, Eq. (26) indicates that the predicted velocity is less than the value of log-law [29]. In other words, Eq. (27) states that for a velocity profile with the maximum velocity below the free surface, the unknown parameter b can be determined from the elevation of the maximum velocity, i.e., $y_{\max}/h$.

The depth-averaged velocity can be obtained by integrating Eq. (25) with respect to y from the bed to the free surface,

$$\frac{b}{\kappa} = \frac{1}{\kappa}\left(\ln\frac{h}{y_0} - 1\right) - \frac{V}{u_*} \tag{28}$$

where V is the depth-averaged velocity. The first term of right-hand-side in Eq. (28) is the theoretical depth-averaged velocity as predicted by the classical log-law. Thus Eq. (28) states that the unknown parameter b can be evaluated by the velocity defect between the measured mean velocity (V/u_*) and the depth-averaged velocities as given by the classical log-law.

Strictly speaking, the vertical velocity $\bar{v}$ is not zero even in steady and uniform flows. The non-zero vertical velocity $\bar{v}$ in steady channel flows has been detected since Prandtl's era. The experimental results by Nezu and Nakagawa [15] show that $\bar{v} \neq 0$ due to the secondary currents which, for narrow channel (channel width/water depth < 5) are initiated by the sidewall effect, free surface effect or the variation of bed topology, for shallow-wide channel or 2-D flow, the non-zero $\bar{v}$ or secondary currents can be generalized by the variation of lateral bed topology and the corner secondary currents [26]. It is natural that the wall-normal velocity in the non-uniform and unsteady flows can be further induced by many factors, such as the unsteadiness, non-uniformity, sediment concentration, and temperature gradient [28] etc. It is worthwhile to investigate the impact of wall-normal velocity $\bar{v}$ on the streamwise velocity. In practice any type of wall-normal velocity profile is possible, and numerical integration may be necessary to obtain the streamwise velocity distribution using Eq. (24) if the profile of $\bar{v}$ is given. This study only provides simple examples to demonstrate how one could assess the influence of wall-normal velocity on the streamwise velocity by assuming the wall-normal velocity in the following form:

$$\frac{\bar{v}}{u_*} = \alpha\kappa\xi^n(1-\xi)^m \tag{29}$$

where α, n and m are coefficients to be determined. Eq. (29) states that at the bed where $\xi = 0$, $\bar{v} = 0$; at the mean surface level where $\xi = 1$, Eq. (29) gives $\bar{v} = 0$. By substituting Eq. (29) into (24), one can obtain a simple velocity distribution for any given values of α, n and m. For simplicity, we assume $n = m = 1$.

By substituting Eq. (29) into Eq. (24), one has

$$\frac{\bar{u}}{u_*} = \mathrm{e}^{\alpha\xi}\left[\frac{1}{\kappa}\int\frac{\mathrm{e}^{-\alpha\xi}}{\xi}\,\mathrm{d}\xi + \frac{b}{k}\int\frac{\mathrm{e}^{-\alpha\xi}}{1-\xi}\,\mathrm{d}\xi + c\right] \tag{30}$$

The first and second terms in the bracket of Eq. (30) can be approximately calculated using the Taylor series and only the first three terms are used:

$$\int \frac{e^{-\alpha\xi}}{\xi}\,d\xi \approx \int \left(\frac{1}{\xi} - \alpha + \frac{1}{2}\alpha^2\xi\right) d\xi = \ln\xi - \alpha\xi + \left(\frac{\alpha\xi}{2}\right)^2 \tag{31}$$

$$\int \frac{e^{-\alpha\xi}}{1-\xi}\,d\xi = -e^{-\alpha}\int \frac{e^{\alpha(1-\xi)}}{1-\xi}\,d(1-\xi) \approx -e^{-\alpha}\left(\ln(1-\xi) + \alpha(1-\xi) + \left(\alpha\frac{1-\xi}{2}\right)^2\right) \tag{32}$$

Using the non-slip boundary condition at $\xi = \xi_0$, and $\xi_0 \ll 1$, $\bar{u} = 0$, the integration constant c can be determined as follows:

$$c = \frac{b}{\kappa}e^{-\alpha}\left(\frac{\alpha^2}{4} - \alpha\right) - \frac{1}{\kappa}\ln\xi_0 \tag{33}$$

therefore, it can be seen that all parameters, such as the bed roughness (Δ), the channel bed slope ($\sin\theta$), the non-uniformity (dh/dx), the Reynolds shear stress caused by velocity fluctuations ($-\overline{u'v'}$), the shear stress caused by mean velocities ($\bar{u}\bar{v}$) as well as the shear stress induced by waves ($\tilde{\tilde{u}}\tilde{\tilde{v}}$) jointly influence the velocity profile. These parameters can be included or reflected in the following equation of velocity distribution by substituting Eqs. (31)–(33) into Eq. (30).

$$\frac{\bar{u}}{u_*} = \frac{1}{\kappa}e^{\alpha\xi}\left\{\ln\frac{y}{y_0} - \alpha\xi + \left(\frac{\alpha\xi}{2}\right)^2 - be^{-\alpha}\left[\ln(1-\xi) + \alpha(1-\xi) + \left(\alpha\frac{1-\xi}{2}\right)^2 - \frac{\alpha^2}{4} + \alpha\right]\right\} \tag{34}$$

It is obvious that Eq. (34) becomes Eq. (25) if $\alpha = 0$, and Eq. (34) becomes Eq. (26) if $b = \alpha = 0$.

4. Comparison with Kemp and Simons' experimental data

Several laboratory measurements of velocity profiles are available. One of the widely cited measurements was that of Kemp and Simons [9,10], who measured velocities in laboratory channels with rough and smooth beds using LDA. The mean velocity profiles were measured in a square channel 10.06 m long and 0.475 m in width and depth. The bed roughness was represented by 5 mm high triangular wooden strips placed at 18 mm intervals along the channel bed. The incident wave is set to propagate against the direction of the currents. The flow depth at the test section was kept at 200 mm for all tests. Regular waves were generated with a constant wave period of 1 s. The wave height varied from 27.9 to 59.1 mm, and the wave length varied from 1053 mm to 1055 mm. The measured and computed velocities are shown in Fig. 2. The measured velocity profiles of waves propagating with the current over a smooth bed are shown in Fig. 3. Eqs. (25), (26) and (34) are included for comparison. All basic parameters are listed in Table 1.

In Table 1, the shear velocity u_* and y_0 are obtained by best fitting the near bed velocity with the classical log-law. The coefficients α and b are determined by best fitting the measured over-all velocity with Eqs. (25) and (34).

It can be seen from Fig. 2 that Eqs. (25) and (34) yield similar results and both are very close to the measured data. Eq. (26) or the universal log-law is only valid near the bed. Fig. 3 shows that the maximum velocity appears below the free surface, and Eq. (34) represents

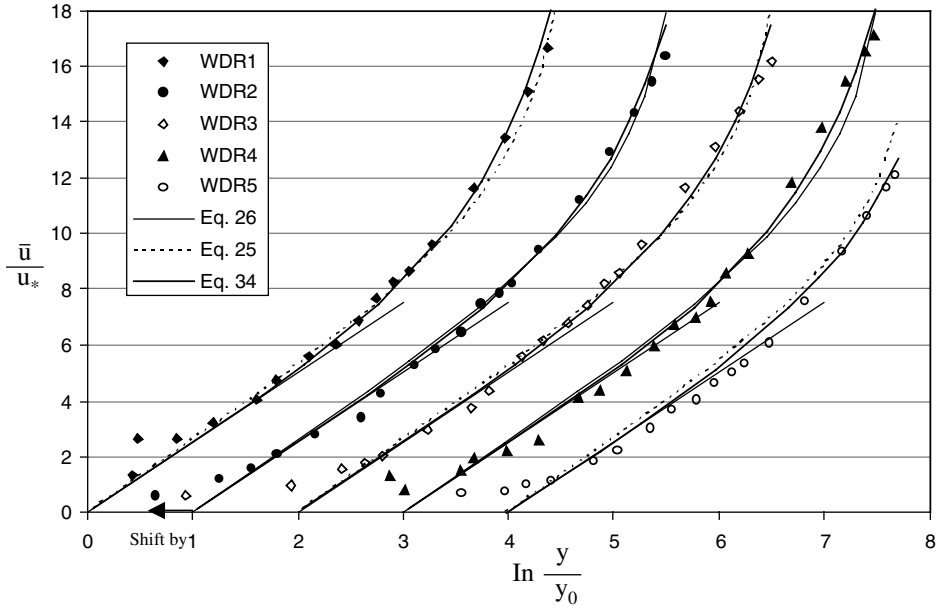

Fig. 2. Comparison of measured velocity profiles with Eqs. (25), (26) and (34) for waves opposing currents over a rough bed.

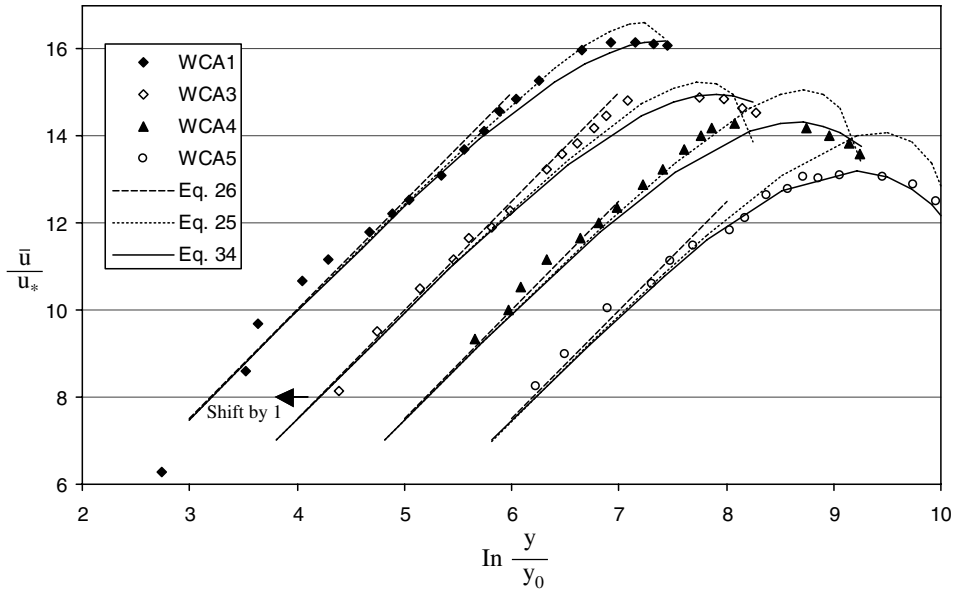

Fig. 3. Comparison of measured velocity profiles with Eqs. (25), (26) and (34) for waves following currents over a smooth bed.

Table 1
Parameters for velocity profiles shown in Figs. 2 and 3

	WDR1	WDR2	WDR3	WDR4	WDR5	WCA1	WCA2	WCA3	WCA4
Wave height (mm)	27.9	33.4	39.7	50.5	59.1	20.7	30.7	39.4	44.4
Wave length (mm)	1053	1055	1055	1055	1055	1426	1425	1430	1433
Wave period (s)	1.003	1.003	1.003	1.003	1.003	1.006	1.006	1.006	1.006
Water depth (mm)	200	200	200	200	200	200	200	200	200
u_* (mm/s)	8.52	9.52	10	10	14.3	15	17	17.5	18.5
y_0 (mm)	1.9	1.9	1.9	1.9	4.2	0.1	0.12	0.12	0.12
b (Eq. (25))	1.6	1.4	1.4	1.4	1	−0.5	−0.9	−1	−1.7
α (Eq. (34))	0.8	0.65	0.65	0.7	0.5	−0.19	−0.28	−0.38	−0.65
Remarks	Waves opposing current, rough bed					Waves following current, smooth bed			

the velocity profiles slightly better than Eq. (25) when the simple distribution of vertical velocity is given in Eq. (29). More precise measurements are needed to identify whether $b \neq 0$ or $\bar{v} \neq 0$ causes the deviation of the measured velocity from the classical log-law. Table 1 shows that b and α are positive when waves propagate against the current, but they become negative when waves propagate in the direction of the current.

5. Comparison with other experimental data

Van Rijn et al. [23] measured the velocity distribution in a channel 45 m long, 0.8 m wide and 1.0 m deep. A horizontal sand bed was installed (length 25 m, thickness 0.1 m). Fine sand of 0.2 mm median grain size was used. The water-level variations were measured using a resistance probe near the test section. The velocities were measured using an electromagnetic velocity meter with a measuring volume of about $3 \times 3 \times 3$ mm^3 below the probe. The water depth was about 0.5 m, wave period was about 2.5 s. The measured velocities are shown in Figs. 4–7 in which H_s is the significant wave height; b and α are determined by best fitting the measured velocity profile near the free surface (see

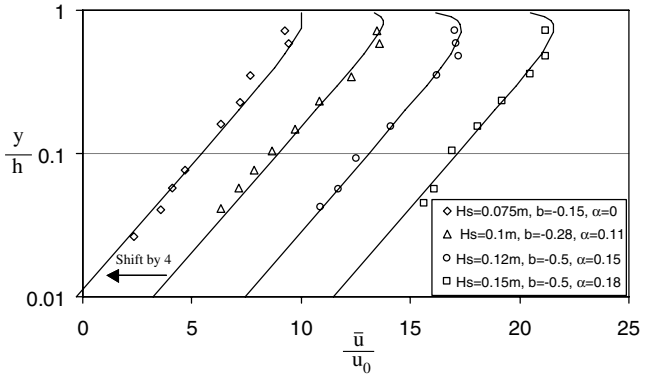

Fig. 4. A comparison between Van Rijn et al. [23] experimental data (mean velocity = 0.2 m/s) and predicted results: waves following currents.

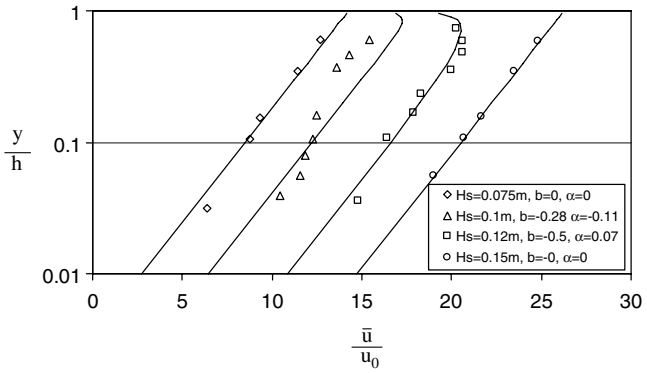

Fig. 5. A comparison between Van Rijn et al. [23] experimental data (mean velocity = 0.4 m/s) and predicted results: waves following currents.

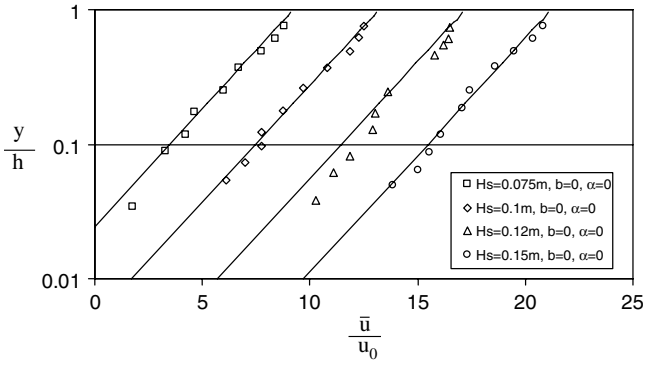

Fig. 6. A comparison between Van Rijn et al. [23] experimental data (mean velocity = 0.2 m/s) and predicted results: waves opposing currents.

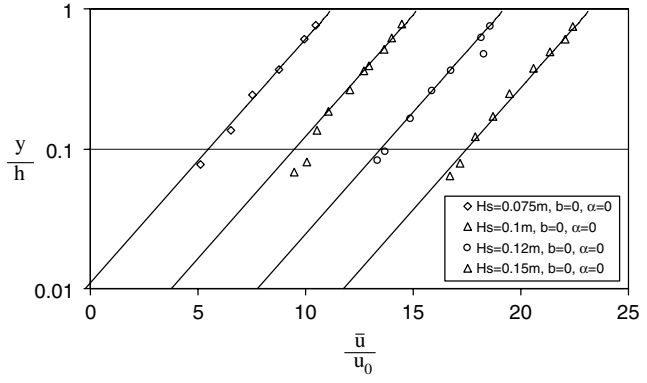

Fig. 7. A comparison between van Rijn et al experimental data (mean velocity = 0.4 m/s) and predicted results: waves opposing currents.

Table 2). The figures show good agreement between Eq. (34) and the measured results.

Figs. 4–7 show the velocity profiles under waves in combination with co-flowing and opposing currents. It can be seen that in some cases b and α are zero, but in some cases non-zero values are obtained. To demonstrate the influence of wave–current angle on velocity

Table 2
Basic parameters for velocity profiles

Author	Van Rijn et al. [23]																Van Rijn and Havinga [25]			
Water depth (cm)	50	50	50	50	50	50	50	50	50	50	50	50	50	50	50	50	40	40	40	40
Mean velocity (cm/s)	20	20	20	40	40	40	20	20	20	20	0.2	40	40	40	40	40	10	10	10	10
Wave height (mm)	75	100	120	150	75	100	120	150	75	100	120	150	75	100	120	150	70	100	100	140
Wave period (s)	2.5	2.5	2.5	2.5	2.5	2.5	2.5	2.5	2.5	2.5	2.5	2.5	2.5	2.5	2.5	2.5	2.5	2.5	2.5	2.5
u_* (mm/s)	25	25	25	35	25	40	35	35	30	30	30	30	45	45	45	45	1.2	1.2	1.2	1.2
h/y_0	90	70	70	300	75	250	300	300	40	40	40	40	90	90	90	90	120	400	350	
b (Eq. (25))	−0.15	−0.28	−0.5	−0.5	0	−0.28	−0.5	0	0	0	0	0	0	0	0	0	−0.3	−0.6	−0.6	
α (Eq. (34))	0	0.11	0.15	0.18	0	−0.11	0.07	0	0	0	0	0	0	0	0	0	−0.1	0.35	0.35	
Remarks	Wave following current						Wave following current				Wave opposing current						Angles: 60°, 90° and 120°			

distributions, Van Rijn and Havinga [25] carried out experiments in a wave–current basin, in which the water depth was about 0.4 m in all tests. Three different wave conditions were performed with significant wave height of 0.07 m, 0.1 m and 0.14 m for three wave directions—60°, 90° and 120° between wave orthogonal and current direction. Irregular waves with a single-topped spectrum and peak period of 2.5 s were generated. Instantaneous fluid velocities were measured by an acoustical probe and an electromagnetic probe. Fig. 8 displays good agreement between the measured and calculated velocity profiles using Eq. (34).

The present model has also been compared with the laboratory measurements of Van der Kaaij and Nieuwjaar [22]; Kampen and Nap [24] and Klopman [12] in Figs. 9–12, in which S1510, T1210, T1810 and CMP refer to the waves following the currents and S15-10, T12-10, T18-10 and CMP refer to the waves opposing currents.

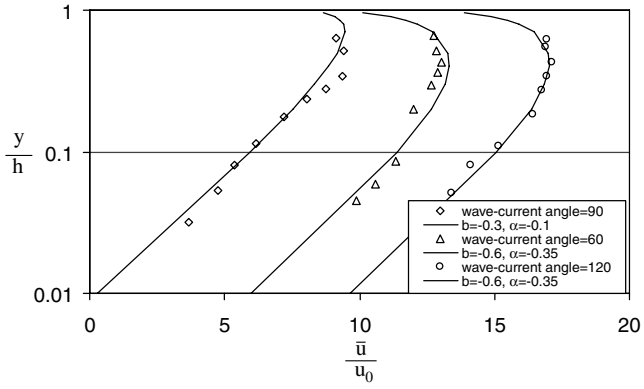

Fig. 8. Influence of wave–current angle on velocity profile.

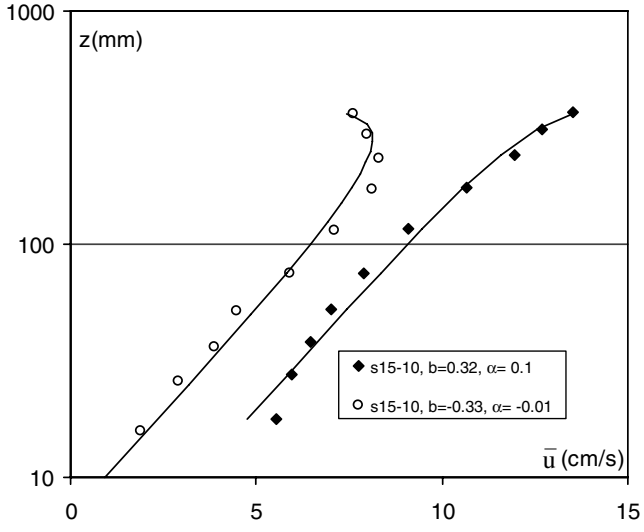

Fig. 9. Comparison of Eq. (34) with van Kampen and Nap [24].

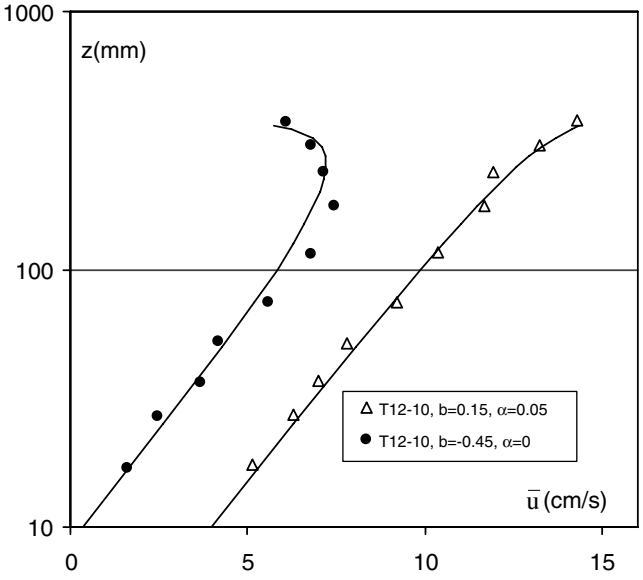

Fig. 10. Comparison of Eq. (34) with Van der Kaaij and Nieuwjaar's [22] experimental data.

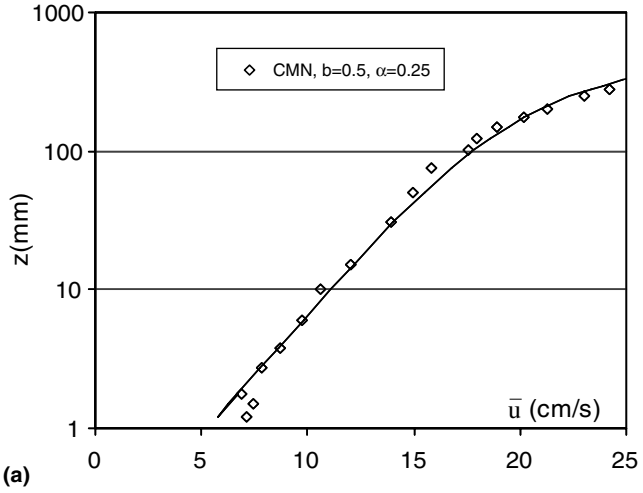

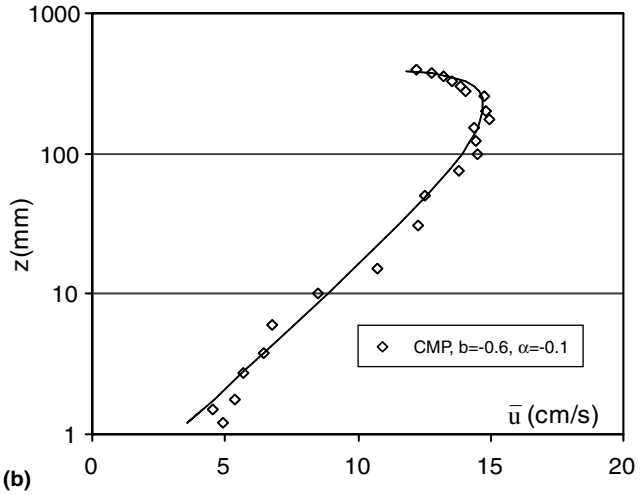

Fig. 11. Comparison of Eq. (34) with Kampen and Nap's experimental data.

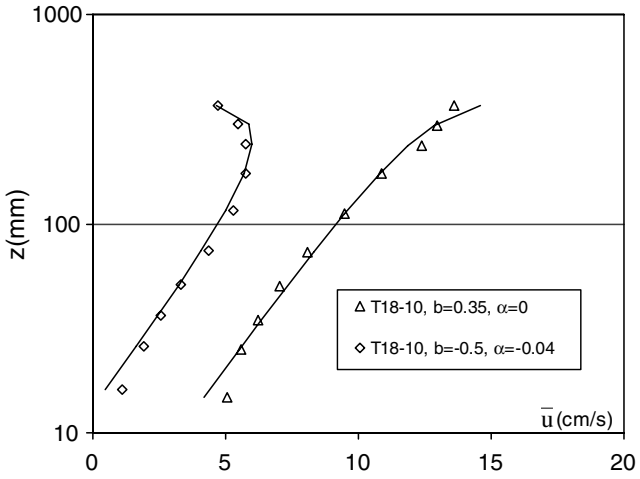

Fig. 12. Comparison of Eq. (34) with Klopman's experimental data.

6. Discussion on the non-zero wall-normal velocity and Reynolds shear stress

When the present model is applied to estimate the velocity distribution in combined wave–current flows, two parameters i.e., b and α should be determined. The former indicates that the Reynolds shear stress in the wave–current flows deviates from the standard linear distribution in the circular pipe flows (2-D flows); the latter actually expresses the magnitude of vertical velocity. Therefore, it is necessary to analyze (i) why the momentum equation shown in Eq. (22) differs from the well-known standard-linear relationship; (ii) whether the wall-normal velocity is zero, and (iii) the validity of the Reynolds stress model, i.e., Eq. (23b).

Theoretically, b is determined by the following equation:

$$b = 1 - \frac{gh(\sin\theta + S)}{u_*^2} - \frac{ah}{u_*^2} \tag{35}$$

In order to assess the parameter b, flows with the presence of wave in the steady and uniform open channels (time-averaged velocities kept constant in the streamwise direction, i.e., $\partial Q/\partial x = 0$ or $\mathrm{d}h/\mathrm{d}x = 0$) are discussed first. From Eq. (19), $S = 0$, then

$$b = 1 - \frac{g\sin\theta + a}{u_*^2}h \tag{36}$$

If the experiments were conducted in horizontal channels or basins where $\sin\theta = 0$, the kinetic energy must be dissipated along x-direction to maintain the flow movement. Then $\mathrm{d}h/\mathrm{d}x$ must be greater than zero or $S > 0$. Eq. (35) becomes

$$b = 1 - \frac{gS + a}{u_*^2}h \tag{37}$$

Eqs. (36) and (37) indicate that the parameter b can be affected by the channel slope $\sin\theta$. In order to determine b, one has to know the channel bed slope, unfortunately this parameter was not measured in the experiments shown in the literature. Also, according to Eq. (22) the wall-normal velocity also plays an important role to the deviation of Reynolds shear stress from the standard linear relationship. Even in the steady and uniform flows, it is well known that the secondary currents are formed in open channel flows, and it is widely agreed that the secondary currents result in the distortion of velocity profiles from the classical log-law [15]. It is also expected that the secondary currents in the combined wave–current flow differ from that in flows without wave presence.

On the other hand, the experiments shown in the above section were virtually conducted in the non-uniform flows ($\mathrm{d}h/\mathrm{d}x \neq 0$) in which the wall-normal velocity and the parameter b are closely related because the vertical velocity on the free surface is non-zero and is given by

$$\bar{v}_{y=h} = \bar{u}_{y=h}\frac{\mathrm{d}h}{\mathrm{d}x} \tag{38}$$

where $\bar{v}_{y=h}$ and $\bar{u}_{y=h}$ are wall-normal and streamwise velocities at the free surface. For accelerating flows $\mathrm{d}h/\mathrm{d}x < 0$, then $\bar{v}_{y=h} < 0$; for decelerating flows, $\mathrm{d}h/\mathrm{d}x > 0$, then $\bar{v}_{y=h} > 0$. Substituting the free surface boundary condition at $\xi = 1, \overline{u'v'} = 0$ into Eq. (22), one gets

$$b = -\frac{\bar{u}_{\xi=1}\bar{v}_{\xi=1}}{u_*^2} \tag{39}$$

for uniform flows where $\mathrm{d}h/\mathrm{d}x = 0$ or $\bar{v}_{\xi=1} = 0$, then $b = 0$, Eq. (22) states that the influence of wave on the velocity profile vanishes, which differs from previous studies, such as the work done by You [30] who claimed that the influence of wave on the velocity profile always exists regardless of flow uniformity, and according to their theory it is impossible that, in any cases the measured velocity in wave–current flows follows the log-law.

However, Figs. 6 and 7 confirm that the measured velocity profiles still follow the log-law, this indicates clearly that the shear stress induced by wave (or $\overline{\tilde{u}\tilde{v}}$) is not the sole factor that causes the deviation of measured velocity profiles from the log-law, the flow's non-uniformity is also responsible for this deviation. The latter can be seen clearly from the measured results [21] in a non-uniform flow without surface waves.

Song [21] measured the velocity and turbulent structure of non-uniform flows using the acoustic doppler velocity profiler (ADVP). The typical mean-velocity $\bar{v}$ and Reynolds shear stress are shown in Figs. 13 and 14. It can be concluded from Figs. 13 and 14 that in non-uniform flows, $\bar{v} \neq 0$ and the non-zero wall-normal velocity $\bar{v}$ can also result in significant deviations of the measured Reynolds shear stress shown in Fig. 14, i.e.,

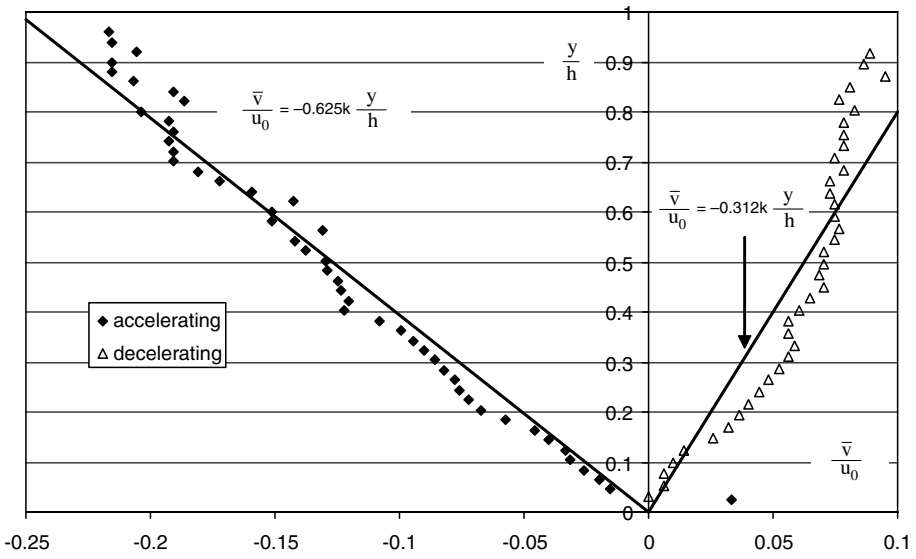

Fig. 13. Distributions of measured vertical velocity in accelerating and decelerating flows based on Song's experimental data (accelerating flow AS00-Q145; decelerating flow DS75-Q60).

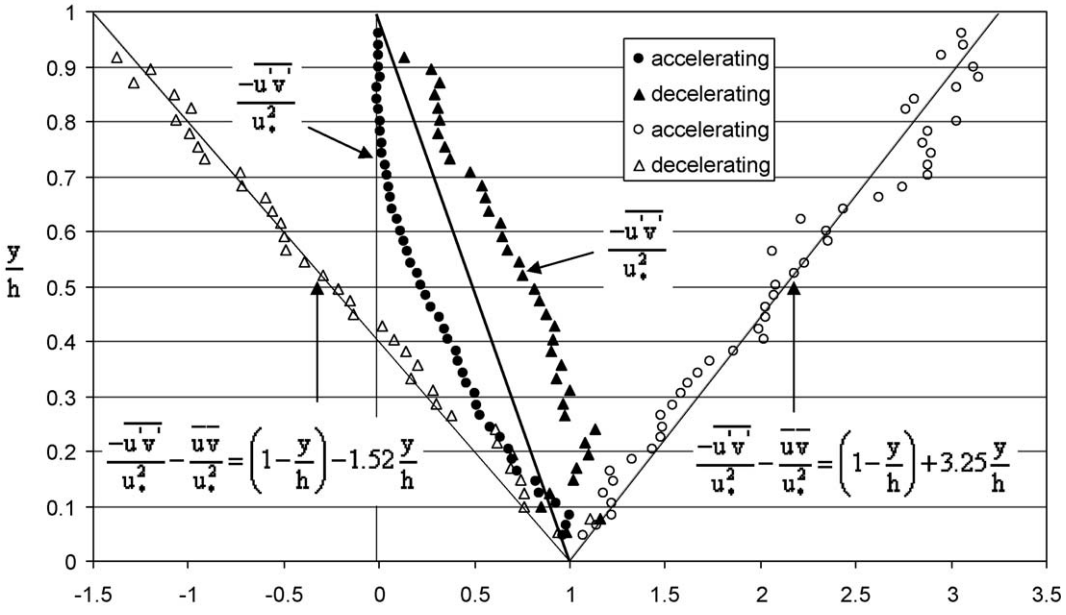

Fig. 14. Reynolds shear stress distributions in accelerating and decelerating flows based on Song's experimental data (accelerating flow AS00-Q145; decelerating flow DS75-Q60).

$$\frac{-\overline{u'v'}}{u_*^2} = 1 - \xi \tag{40}$$

Fig. 14 plots the distribution of $(-\overline{u'v'} - \bar{u}\bar{v})/u_*^2$ against y/h, in which the measured $\overline{u'v'}$, $\bar{u}$ and $\bar{v}$ are used. A linear relationship between $(-\overline{u'v'} - \bar{u}\bar{v})/u_*^2$ and y/h can be found and it indicates that $b > 0$ for accelerating flows and $b < 0$ for decelerating flows. Thus, it can be concluded from Figs. 13 and 14 that in non-uniform flows, the coefficient b and wall-normal velocity are non-zero. Therefore, we may conclude that the theoretical determination of non-zero b and α in the model will be more difficult for flows with the combination of wave and current than that in pure non-uniform flows.

In this model, the Reynolds shear stress is modeled using an empirical equation (Eq. (23b)). It is useful to discuss the validity of Eq. (23b). Unfortunately, we also did not find any relevant measurement/data in the literature. Fig. 15 shows the measured dimensionless Reynolds shear stress $\frac{\overline{u'v'}}{u_*^2}/(\frac{d\bar{u}/u_*}{d\xi})$ against ξ for different flow cases including the accelerating/decelerating flows based on Song's [21] experimental data, and the

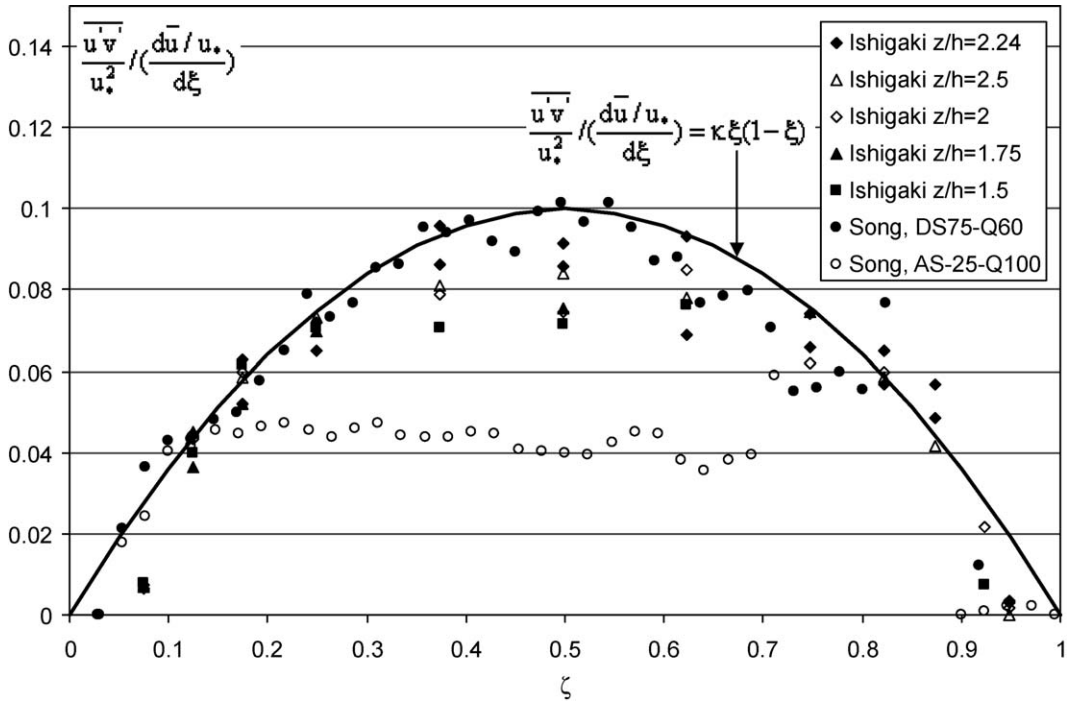

Fig. 15. Measured dimensionless Reynolds shear stress distributions.

steady and uniform flows based on Ishigaki's experimental data.

It is seen from Fig. 15 that the Reynolds shear stress in steady and uniform channel flows can be roughly modeled by the following equation:

$$\frac{\overline{u'v'}}{u_*^2}\Big/\left(\frac{\mathrm{d}\bar{u}/u_*}{\mathrm{d}\xi}\right) = \kappa\xi(1-\xi) \tag{41}$$

Fig. 15 shows that the measured dimensionless Reynolds shear in the middle zone ($0.25 < \xi < 0.75$) tends to be constant rather than a peak value at $\xi = 0.5$. For accelerating flows (Song, AS-25-Q100), the dimensionless Reynolds shear stress is constant in the middle zone ($0.25 < \xi < 0.75$), but the decelerating flow (Song, DS75-Q60) displays good agreement with the model. All data shown in Fig. 15 indicate that the model provides good agreement in two end cases: one is near the boundary and the other near the free surface. Thus, Fig. 15 states that the Reynolds shear stress used in this study, i.e., Eq. (41) or Eq. (23b) is only a first-order-approximation. It is recommended that further investigation be focused on refining the model for Reynolds shear stress under different conditions.

In this study, the empirical parameters b and α are estimated by best-fitting technique, no attempt is made to estimates priorly these values or to generalize the results because b and α involve in the non-uniformity of the mean flow ($\mathrm{d}h/\mathrm{d}x$) and bed slopes ($\sin\theta$), in literature the basic information was not measured. Thus, the writers are unable to develop empirical equations to estimate b and α, but it is clear from this study that the velocity deviation from log-law in combined wave–current flows can be ascribed to the shear stresses $\bar{u}\bar{v}$ and $\overline{\tilde{u}\tilde{v}}$ caused by mean velocities and waves, respectively.

7. Conclusions

The Reynolds equations in the combined wave–current flows are derived from Navier–Stokes equations, and the simplified form of Reynolds shear stress in the 2-D flows is established. The theoretical results show that the Reynolds shear stress in the combined wave–current flow differs from that in steady channel flows for the former is influenced by the flow's uniformity, wave-induced Reynolds shear stress as well as the non-zero wall-normal velocity. The theoretical velocity distribution in wave–current flows is obtained by solving the Reynolds equation using the simplified mixing-length hypothesis. The model is compared with measured velocity profiles available in the literature and good agreement is achieved. Finally, the investigation shows that secondary currents, flow's uniformity, waves greatly affect the velocity profile, and then lead to the deviation of the measured velocity from the classical log-law, this conclusion is quite different from the prevailing view that the wave Reynolds shear stress is a single factor for the velocity deviation from the log-law.

However, due to lack of the exact geometrical and flow information in the published papers, such as the bed slope, variation of water depth, etc., it is impossible for the writers to develop empirical equations to

estimate the parameters b and α involved in terms of independent flow and wave parameters, thus further systematical experiments are needed in next stage.

References

[1] Anwar HO, Atkins R. Turbulence measurements in simulated tidal flow. J Hydr Div ASCE 1980;106(8):1237–89.

[2] Christoffersen JB, Jonsson IG. Bed friction and dissipation in a combined current and wave motion. Ocean Eng 1985;12:387–423.

[3] Coles D. The law of the wake in the turbulent boundary layer. J Fluid Mech 1956;1:191–226.

[4] Fredsoe J. Turbulent boundary layers in wave–current motion. J Hydr Eng ASCE 1984;110:1103–20.

[5] Grant WD, Madsen OS. Combined wave current interaction with a rough bottom. J Geophys Res 1979;84:1797–808.

[6] Groeneweg J, Klopman G. Changes of the mean velocity profiles in the combined wave–current motion described in a GLM formulation. J Fluid Mech 1998;370:271–96.

[7] Groeneweg J, Battjes JA. Three-dimensional wave effects on a steady current. J Fluid Mech 2003;478:325–43.

[8] Immamoto H, Ishigaki T. Measurement of secondary flow in an open channel. In: Proc of 6th IAHR-APD cong, Kyoto, Japan, 1988, p. 513–20.

[9] Kemp PH, Simons RR. The interaction between waves and a turbulent current: waves propagating with the current. J Fluid Mech 1982;116:227–50.

[10] Kemp PH, Simons RR. The interaction of waves and turbulent current: waves propagating against the current. J Fluid Mech 1983;130:73–89.

[11] Keulegan CH. Laws of turbulence flow in open channels. J Res The Nat Bur Standards 1938;21:707–40.

[12] Klopman G. Vertical structure of the flow due to waves and currents. Delft Hydraulics Laboratory, Report H840, Part II, 1994.

[13] Longuet-Hinggins MS. The mechanics of the boundary layer near the bottom in a progressive wave. In: Proc 6th int conf coastal eng, Miami, 1956, p. 184–93.

[14] Lundgren H. Turbulent currents in the presence of waves. In: Proc. 13th int conf coastal eng. Vancouver, 1972, p. 623–34.

[15] Nezu I, Nakagawa H. Turbulence in open channel flows. Monograph series of IAHR. Rotterdam, Netherland: A.A. Balkema; 1993.

[16] Nielsen P, You ZJ. Eulerian mean velocities under non-breaking waves. In: Proc 25th int conf coastal eng, Florida, 1996.

[17] Rivero FJ, Arcilla AS. On the vertical distribution of $\overline{\tilde{u}\tilde{v}}$. Coastal Eng 1995;25:137–52.

[18] Rivero FJ, Arcilla AS. On the vertical distribution of $\overline{\tilde{u}\tilde{v}}$: reply to the comments of Z.J. You. Coastal Eng 1997;30:311–5.

[19] Sherman D, Greenwood B. Boundary roughness and bed forms in the surf zone. Mar Geol 1984;60:199–218.

[20] Sleath JD. Velocities and shear stress in wave–current flows. J Geophys Res 1991;96:15237–44.

[21] Song TC. Velocity and turbulence distribution in non-uniform and unsteady open-channel flow. PhD thesis, Ecole Polytechnique Federale De Lausanne, 1994.

[22] Van der Kaaij Th, Nieuwjaar MWC. Sediment concentration and sediment transport in case of irregular non-breaking waves with a current. Faculty of civil Engineering, Delft University of Technology, 1987.

[23] Van Rijn LC, Nieuwjaar MWC, Kaay TVD, Nap E, Van Kampen A. Transport of fine sands by currents and waves. J Waterway, Port, Coastal Ocean Eng 1993;119(2):123–43.

[24] van Kampen HFA, Nap EN. Sediment concentrations and sediment transport in case of irregular non-breaking waves with current. Faculty of Civil Engineering, Delft University of Technology, 1988.

[25] Van Rijn LC, Havinga FJ. Transport of fine sands by currents and waves. Part II. J Waterway, Port, Coastal Ocean Eng 1995;121(2):123–33.

[26] Wang ZQ, Cheng NS. Secondary flows over artificial bed strips. Adv Water Resour 2005;28:441–50.

[27] Yalin MS. Mechanism of sediment transport. 2nd ed. New York: Pergamon; 1977.

[28] Yang SQ. In: Proc of 13th IAHR-APD congress on 1st and 2nd order approximate solutions of Reynolds equations in 3-D channels. Singapore: World Scientific; 2002.

[29] Yang SQ, Tan SKt, Lim SY. Velocity distribution and dip phenomena in smooth and straight open channel flow. J Hydraul Eng ASCE 2004;130(12):1179–86.

[30] You ZJ. The effect of wave-induced stress on current profiles. Ocean Eng 1997;23:619–28.